Fisher, A., Davis, E.E., and Escutia, C. (Eds.), 2000
Proceedings of the Ocean Drilling Program, Scientific Results, Vol. 168

11. PETROGRAPHY AND CHEMICAL COMPOSITIONS OF SECONDARY CALCITE AND ARAGONITE IN JUAN DE FUCA RIDGE BASALTS ALTERED AT LOW TEMPERATURE[1]

Autumn Yatabe,[2] David A. Vanko,[2,3] and A. Mohamad Ghazi[2]

ABSTRACT

During Leg 168 a transect was drilled across the eastern flank of the Juan de Fuca Ridge in an area where the volcanic basement is covered by sediments of variable thickness. Samples of basement volcanic rocks were recovered from nine locations along the transect, where the basement sediment interface is presently heated to temperatures varying from 15° to 64°C. Altered rocks with secondary calcium carbonate were common at four of the sites, where present-day temperatures range from 38° to 64°C. Fluid inclusions in aragonite suggest that the mineral precipitated from an aqueous fluid of seawater salinity at temperatures well below 100°C.

The chemical compositions of secondary calcite and aragonite were determined with both an electron microprobe and a laser-ablation inductively coupled plasma-mass spectroscopy (LA–ICP-MS) microprobe. These two techniques yielded consistent analyses of the same minor elements (Mg and Sr) in the same specimens. The combined results show that secondary aragonites contain very little Mg, Mn, Fe, Co, Ni, Cu, Zn, Rb, La, Ce, Pb, or U, yet they contain significant Sr. In contrast, secondary calcites contain significant Mg, Mn, Fe, Ni, Cu, Zn, and Pb, yet very little Co, Rb, Sr, La, Ce, or U. Secondary calcium carbonates provide subseafloor reservoirs for some minor and trace elements. Replacement of aragonite by calcite should result in a release of Sr, Rb, and Zn to solution, and it provides a sink for Mg, Mn, Ni, Cu, Zn, and Pb.

INTRODUCTION

The circulation of low-temperature (<150°C) hydrothermal fluids through the flanks of spreading ridges has important physical and chemical consequences on a global scale (Sclater et al., 1976; Anderson et al., 1977; Alt et al., 1986; Purdy, 1987; Mottl and Wheat, 1994; Stein and Stein, 1994). Chemical fluxes from low-temperature alteration of mid-ocean ridge basalts (MORBs) could be important in crust as old as 10 Ma or more, or as long as significant ridge-flank fluid flow occurs (Hart and Staudigel, 1986; Mottl and Wheat, 1994). Ocean Drilling Program (ODP) Leg 168 was dedicated to studying ridge-flank hydrothermal processes near the Juan de Fuca Ridge (Davis, Fisher, Firth, et al., 1997). This paper reports on the role played by secondary carbonate minerals in the low-temperature hydrothermal alteration of MORB recovered during Leg 168 on the eastern flank of the Juan de Fuca Ridge (JdFR). Calcite and aragonite formed at temperatures below 64°C are widely distributed in various host lithologies, although they are not ubiquitous. The compositions of calcite and aragonite differ significantly in their trace elements, resulting partly from crystallochemical controls and partly from controls imposed by the solution chemistry.

ANALYTICAL METHODS

Twenty-one small fragile specimens, typically 2–4 cm^3, each containing a single 0.5- to 2-mm-wide carbonate vein, were stabilized with epoxy and then slabbed and fabricated into polished thin sections for standard petrographic analysis. Each section was studied using both regular petrographic microscopes and a Nuclide ELM-3R luminoscope, which induced cathodoluminescence (CL) by means of a cold-cathode discharge tube operated at up to 30-kV accelerating potential and 0.5-mA beam current. For the carbonates, a potential of 15 kV was typical and sufficient to excite intense luminescence. Photomicrographs showing CL were recorded on Ektachrome or Kodak Gold film with exposure times of about 60 s.

Electron microprobe analyses, all located precisely with the aid of CL photographs, were obtained using the JEOL 866 wavelength-dispersive instrument located at the University of Georgia in Athens, Georgia. Analyses were performed with 15-kV accelerating voltage, 5-na beam current, and 10-µm beam diameter and were calibrated using the following natural standards obtained from the Smithsonian museum: calcite = Ca, dolomite = Mg, siderite = Fe and Mn, and strontianite = Sr. Results are recalculated into carbonate molecules assuming all cations are balanced by CO_3^{2-}, and resulting totals within about 3% of 100% were deemed acceptable for our characterization of the major and minor element concentrations.

Four specimens were selected for reconnaissance determinations of a suite of minor and trace elements by laser-ablation inductively coupled plasma-mass spectroscopy (LA–ICP-MS), using the Finnigan MAT Sola ICP-MS equipped with a Nd:YAG laser at Georgia State University, Atlanta, Georgia. Special polished thick sections were prepared for these analyses, typically several hundred micrometers thick. The laser used for microsample ablation operates at 266 nm in the UV region and was operated in the Q-switched mode at 4 Hz repetition and with 4 mJ per pulse. The laser was focused on the carbonate sample surface and produced an ablation pit with a diameter of about 30–40 µm and about 20 µm deep. An argon stream introduced the ablated material as a wet plasma into the ICP torch, and the quadrupole mass spectrometer was set to acquire data continuously during three scans (over about 20 s) using a secondary electron multiplier detector.

Quantification for LA–ICP-MS was accomplished using the National Institute of Standards and Technology standard reference material 611 (SRM-611), which contains known quantities of numerous trace elements at about 500 ppm. The procedures followed closely those reported by Perkins and Pearce (1995), Kontak and Jackson (1995), and Jenner et al. (1993). Calcium, present in SRM-611 at 12 wt% CaO and in the carbonate samples at 51 wt% CaO, served as an internal standard to correct for differences in the ablation yields between the SRM-611 glass and the carbonate samples. Further analytical details are given in the Appendix.

[1]Fisher, A., Davis, E.E., and Escutia, C. (Eds.), 2000. *Proc. ODP, Sci. Results,* 168: College Station TX (Ocean Drilling Program).
[2]Department of Geology, Georgia State University, Atlanta GA 30303, USA.
[3]Correspondence author: dvanko@gsu.edu

Fluid inclusions were studied using a Fluid, Inc., gas-flow heating and freezing stage calibrated with synthetic inclusions at –56.6°, 0.0°, and +374°C. The ice melting temperatures recorded are accurate to ±0.1°C. Techniques outlined in Goldstein and Reynolds (1994) were followed.

RESULTS

Background

The Leg 168 drilling transect across the eastern flank of the Juan de Fuca Ridge was strategically located to take advantage of the regional geological setting (Fig. 1). Shallow igneous crust formed at the Juan de Fuca ridge axis is quickly cooled so that volcanic rocks on the seafloor approach the ambient bottom temperature of 2°C. As the crust drifts eastward as a result of seafloor spreading at a half-rate of about 29 mm/yr (Johnson and Holmes, 1989; Davis and Currie, 1993), these seafloor rocks are initially cold and unsedimented, in open contact with bottom seawater. However, about 20 km east of the rise axis, where the volcanic rocks are about 600,000 yr old, sediments of the Cascadia Basin derived from North America are observed onlapping the volcanic crust. Further to the east, the volcanic basement, progressively buried beneath more and more sediment, grows slowly warmer and more isolated from unaltered seawater because of the thermal insulation and hydrologic impedance of the sediments (Davis et al., 1992).

The basalt/sediment transition was sampled by coring at nine different locations across the Leg 168 transect. The amount of basement penetration varied from only 1 m at Site 1023 to a maximum of 66 m at Site 1026, and basement recovery varied from <6% at Sites 1023, 1024, and 1026, to 50% or more at Sites 1028, 1029, and 1027. Basement recovery was particularly poor at Site 1023, the westernmost and lowest temperature site in the transect, where only a few small abraded specimens were obtained.

Temperature probe measurements at each site in the transect provided control on the present-day temperature of water–rock interaction. Altered basalts discussed in this paper come from the top of the volcanic basement in these nine boreholes where the present-day temperatures vary from 15° to 64°C (Davis, Fisher, Firth, et al., 1997) and circulation varies from open to closed system. Progressive increases in the amount of hydrothermal alteration of MORB and differences in the observed alteration minerals are related to the increased age, closed-system nature, and alteration temperature of the samples.

Two closely spaced boreholes at the eastern end of the Leg 168 transect (Sites 1026 and 1027) were cored to investigate an area with significant sediment-covered basement relief that promotes localized buoyancy-driven fluid flow within the upper basement. Here, the amount of hydrothermal alteration and the observed alteration minerals differ in response to differences in fluid chemistry and lithology.

Secondary alteration affects all igneous rocks recovered during Leg 168, either as discrete alteration haloes parallel to rock margins or fractures or as pervasive alteration. Secondary minerals, most commonly clays, iron oxyhydroxides, and carbonates, line or fill vesicles, coat fracture surfaces, occur as veins, and replace phenocrysts and groundmass. The total amount of alteration varies widely from about 1 to 24 volume percent secondary minerals, with the more easterly samples, which are warmer, exhibiting the most alteration (Marescotti et al., Chap. 10, this volume).

Calcium carbonate occurs alone or associated with saponite in veins and vesicles and also forms as a replacement of olivine, pyroxene, and plagioclase. The vein widths vary from ~0.5 to 2 mm. Crosscutting relationships with respect to clay veins and haloes surrounding clay veins indicate that the carbonate minerals generally occur late in the alteration sequence. Calcium carbonate has an uneven distribution in the Leg 168 site transect (Fig. 1), being present in the massive basalt from Site 1025, the diabase from Site 1027, the basalt breccia at Site 1026, and the pillow basalts from Sites 1028, 1032, 1026, and 1027. In contrast, the pillow basalts at Sites 1023, 1024, 1025, 1031, and 1029 show no evidence of calcium carbonate mineralization.

The temperatures of present-day water–rock interaction at sites with evidence of carbonate mineralization range from Site 1025 at 38°C to Site 1026/1027 at 64°C (Fig. 1). The apparent absence of carbonate at Sites 1023 and 1024 (15° and 23°C) could result from the low temperature, a hydrothermal fluid that is insufficiently modified

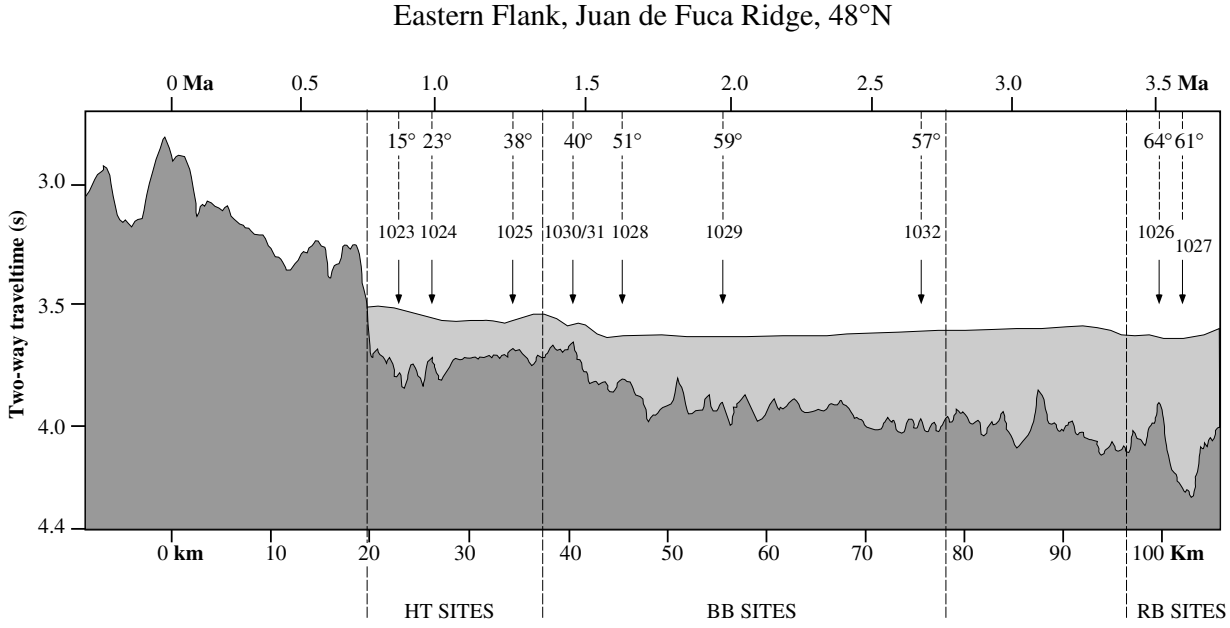

Figure 1. Basement topography (heavily stippled area) and sediment cover (lightly stippled area), across the eastern flank of the Juan de Fuca Ridge at 48°N, derived from composite seismic reflection profiles, from Davis, Fisher, Firth, et al. (1997). The locations of the Leg 168 sites are shown, along with the estimated present-day temperature at the basement/sediment interface. HT = Hydrothermal Transition; BB = Buried Basement; RB = Rough Basement.

from seawater at those two westernmost sites, insufficient time at elevated temperatures, or simply a very low recovery rate.

Petrography

Calcium carbonate exhibits a wide variety of textures observable with either the optical microscope or in cathodoluminescence (CL) (Pls. 1, 2). In veins, the carbonate may occur alone (Pl. 1, Figs. 1, 2, 4) or with saponite (Pl. 2). The carbonate textures vary from blocky (Pl. 1, Figs. 1, 4; Pl. 2) to fibrous (Pl. 1, Fig. 3). The fibrous texture represents a cross-fiber arrangement of parallel elongated crystals with random optical orientations that form as a result of continuous carbonate growth during fracture extension (the classic cross-fiber texture of Ramsay [1980], also discussed in Tartarotti et al. [1996]).

The veins are rarely filled with monomineralic carbonate. There is commonly an intergrowth of calcite and aragonite in individual veins (Pl. 1, Fig. 3) or a change in mineralogy from one polymorph to another along a vein. In many veins, including monomineralic ones, there is commonly intricate compositional zoning as indicated by CL (Pl. 1, Figs. 1, 2, 4; Pl. 2, Figs. 2, 4). For some aragonites that were analyzed by electron microprobe, brighter zones within aragonite crystals commonly contained higher Sr concentrations, so either Sr or another element that covaries with Sr probably serves as CL activators. In calcites, Mn is generally considered to be the main CL activator (Marshall, 1988), although electron microprobe analyses indicate that many other elements are present in Leg 168 calcites, and a simple relationship between CL intensity and Mn concentration does not exist.

When both blocky calcite and fibrous aragonite were observed in single veins within altered basalts from Leg 148 Hole 896A at the Costa Rica Rift, it was suggested that the blocky crystals represented the recrystallization of aragonite to calcite as a result of heating (Tartarotti et al., 1996). This interpretation may also be applicable for the Leg 168 volcanic rocks and could have implications for the storage and release of trace elements during the precipitation of aragonite and any subsequent recrystallization to calcite (see below).

Chemical Compositions

Calcium carbonates from 17 representative specimens were analyzed by electron microprobe. Significantly, all of the analytical microprobe spots were located with the aid of cathodoluminescence photographs. Thus, for each electron microprobe analysis, the calcium carbonate polymorph (calcite or aragonite) is known, because calcite has bright orange CL colors, and aragonite has dull orange and green CL colors (Pls. 1, 2). The analyses for calcite (Table 1) and aragonite (Table 2) exhibit strong systematic differences (Fig. 2). Calcites contain the appreciable minor constituents $MgCO_3$, $MnCO_3$, and $FeCO_3$ (Fig. 2A, B), and, in most cases, the $MnCO_3$ exceeds the other two components. Aragonites, in contrast, typically contain essentially no $MgCO_3$, and very little $MnCO_3$ or $FeCO_3$ (Fig. 2C). These relationships are illustrated for each element individually using frequency histograms (Fig. 3).

Two vein specimens of calcite and two of aragonite were selected for microprobe analysis of trace elements by means of LA–ICP-MS (e.g., Kontak and Jackson, 1995). To assess the accuracy and reproducibility of the LA–ICP-MS technique it was important to choose unzoned samples. Thus, the four specimens selected had been previously determined by electron microprobe and CL studies to be relatively homogeneous. Future experimentation is expected to determine whether minor and trace element differences can be resolved by LA–ICP-MS within specimens that exhibit mineral zoning.

Because electron microprobe and laser-ablation analyses are carried out on different sample preparations (thin sections for the former and thick sections for the latter), it is not possible to analyze the exact spot by both techniques. Nonetheless, independent electron microprobe (Tables 1, 2) and LA–ICP-MS determinations (Table 3) of two minor oxides, MgO and SrO, are very consistent, lending confidence to the LA–ICP-MS technique. Specifically, MgO in calcite from Sample 168-1027B-61X-CC, 29–30 cm (Piece 28), is 0.32 wt% by electron microprobe (EMP), and 0.33–0.45 wt% by LA–ICP-MS. MgO in calcite from Sample 168-1032A-14R-1, 39–46 cm (Piece 10), is 0–1.15 wt% by EMP and 0.15–0.55 wt% by LA–ICP-MS. Strontium oxide in aragonite from Sample 168-1027C-5R-4, 127–130 cm (Piece 9), is 0.19–1.05 wt% by EMP and 0.70–0.91 wt% by LA–ICP-MS. Finally, SrO in aragonite from Sample 168-1027C-5R-6, 47–50 cm (Piece 6), is 0.11–0.37 wt% by EMP and 0.44–0.67 wt% by LA–ICP-MS.

Two values for Pb were determined by LA–ICP-MS, one based on measurement of the ^{206}Pb peak and the other based on ^{208}Pb. There is a systematic error in one (or both) of these determinations, based upon the fact that values derived from the ^{206}Pb peak are uniformly higher. A poor blank correction may be the cause for this uncertainty.

The LA–ICP-MS results illustrate further the significant distinction between the minor and trace element contents of calcite and aragonite (Table 3). In addition to the fact that Fe, Mn, and Mg are enriched in calcites relative to aragonites, a fact previously determined by electron microprobe analysis, the LA–ICP-MS data indicate that calcites contain more Mg, Ni, Cu, Zn, La, Ce, and Pb, relative to aragonites. In contrast, aragonites contain more Sr and Rb relative to calcites.

Fluid Inclusions

Coarse-grained aragonite in Sample 168-1027C-5R-4, 127–130 cm (Piece 9), contains numerous fluid inclusions measuring up to several tens of micrometers in size. Some arrays of inclusions appear to be along healed fractures, and other inclusions are solitary. All inclusions contain liquid only at room temperature, suggesting that the temperature of trapping was well below 100°C (Goldstein and Reynolds, 1994), consistent with present-day temperatures. Vapor bubbles were created artificially by heating polished chips from this sample to 250°C for about 10 min and then quenching to room temperature. Subsequently, freezing experiments were run to determine the vapor-saturated freezing-point depression of the inclusion contents. Fifteen determinations (Fig. 4) gave an average Tm(ice) = –2.1°C (the range was –2.2° to –1.9°C). This matches the expected freezing-point depression of seawater, confirming that the aragonite most likely precipitated from a seawater-derived basement fluid of normal seawater salinity.

DISCUSSION

Calcium carbonate commonly lines fractures or fills nearby vesicles in volcanic specimens from four Leg 168 sites (Sites 1025, 1028, 1032, and 1027), and is absent or only present as a trace mineral in the five other sites (Sites 1023, 1024, 1031, 1029, and 1026). Thermodynamic calculations on basement water compositions indicate that the solutions are oversaturated with respect to calcite at Site 1027, undersaturated with respect to calcite at Site 1031, and more-or-less saturated at the other sites (C. Monin, pers. comm., 1998). This is consistent with the presence of secondary carbonate at Site 1027, its absence at Site 1031, and its irregular distribution in the other Leg 168 sites.

Two Hydrothermal Transition (HT) sites, Sites 1023 and 1024, contain basement water that is close to carbonate saturation (C. Monin, pers. comm., 1998) and that also contains significant alkalinity (M. Mottl, pers. comm., 1998). The apparent absence of aragonite or calcite in samples from these sites, keeping in mind that the recovery was very low, may be because the temperature is too low (15° and 23°C), the basement solution is not modified enough from initial seawater compositions, there has been insufficient time at temperatures elevated above ambient bottom water, or a combination of thermody-

Table 1. Representative electron microprobe analyses of calcite.

Hole, core, section	Piece, interval (cm)	Anl. #	FeO	MnO	MgO	CaO	SrO	Na_2O	Total	$FeCO_3$	$MnCO_3$	$MgCO_3$	$CaCO_3$	$SrCO_3$	Total
1027B-61X-CC	Clast, 28-30	C1	BDL	3.98	0.32	52.65	BDL	0.05	57.00	0.00	6.45	0.67	93.97	0.00	101.09
1027C-1R-2	Pc. 1A, 0-4	C12	0.41	1.31	0.93	52.76	BDL	BDL	55.41	0.66	2.12	1.94	94.17	0.00	98.89
1027C-1R-2	Pc. 1A, 0-4	C13	BDL	0.76	0.23	54.14	BDL	0.05	55.27	0.00	1.23	0.48	96.63	0.00	98.34
1027C-1R-2	Pc. 1A, 0-4	C17	0.32	1.66	0.71	52.44	BDL	0.05	55.18	0.52	2.69	1.48	93.59	0.00	98.28
1027C-1R-2	Pc. 1A, 0-4	C18	0.54	1.65	1.15	51.63	BDL	BDL	55.00	0.87	2.67	2.40	92.15	0.00	98.09
1027C-1R-2	Pc. 1A, 0-4	C19	0.87	2.54	2.94	48.80	BDL	BDL	55.23	1.40	4.12	6.14	87.10	0.00	98.75
1027C-1R-3	Pc. 1A, 45-47	C33	1.19	2.72	4.27	46.52	BDL	BDL	54.79	1.92	4.41	8.91	83.03	0.00	98.27
1027C-1R-3	Pc. 1A, 45-47	C36	0.32	1.64	1.57	51.63	BDL	BDL	55.20	0.52	2.66	3.28	92.15	0.00	98.60
1027C-1R-3	Pc. 1A, 45-47	C52	0.57	2.38	3.30	48.99	BDL	BDL	55.24	0.92	3.86	6.89	87.44	0.00	99.10
1027C-1R-3	Pc. 1A, 45-47	C53	0.56	1.92	2.37	51.30	BDL	BDL	56.21	0.90	3.11	4.95	91.56	0.00	100.52
1027C-1R-4	Pc. 1E, 108-110	C38	BDL	2.07	0.33	53.62	BDL	BDL	56.11	0.00	3.35	0.69	95.70	0.00	99.74
1027C-1R-4	Pc. 1E, 108-110	C39	0.75	2.46	4.04	47.72	BDL	BDL	55.05	1.21	3.99	8.43	85.17	0.00	98.80
1027C-1R-6	Pc. 2, 65-69	C47	0.16	3.44	0.63	50.92	BDL	BDL	55.19	0.26	5.57	1.32	90.88	0.00	98.03
1027C-1R-6	Pc. 2, 65-69	C48	0.74	4.14	1.61	49.92	BDL	BDL	56.45	1.19	6.71	3.36	89.10	0.00	100.36
1027C-1R-6	Pc. 2, 65-69	C49	0.38	5.33	0.59	49.32	BDL	BDL	55.66	0.61	8.64	1.23	88.03	0.00	98.51
1027C-1R-6	Pc. 2, 65-69	C50	0.26	5.87	0.58	48.84	BDL	BDL	55.58	0.42	9.51	1.21	87.17	0.00	98.31
1028A-15X-6	Pc. 2, 130-132	C67	BDL	0.19	0.15	54.80	BDL	BDL	55.29	0.00	0.31	0.31	97.81	0.00	98.43
1028A-15X-6	Pc. 2, 130-132	C74	1.26	3.68	2.80	48.11	BDL	BDL	55.92	2.03	5.96	5.85	85.87	0.00	99.71
1028A-15X-6	Pc. 2, 130-132	C77	1.11	3.40	2.11	49.00	BDL	BDL	55.65	1.79	5.51	4.41	87.45	0.00	99.16
1028A-15X-6	Pc. 2, 130-132	C78	0.85	3.39	1.99	49.62	BDL	0.20	56.14	1.37	5.49	4.15	88.56	0.00	99.58
1028A-15X-6	Pc. 2, 130-132	C79	0.75	2.76	0.85	52.87	BDL	0.05	57.28	1.21	4.47	1.77	94.36	0.00	101.82
1028A-15X-6	Pc. 2, 130-132	C82	1.36	3.78	2.03	48.54	BDL	0.05	55.76	2.19	6.13	4.24	86.63	0.00	99.19
1028A-15X-6	Pc. 2, 130-132	C136	0.20	0.30	0.87	53.99	BDL	BDL	55.36	0.32	0.49	1.82	96.36	0.00	98.98
1028A-15X-6	Pc. 2, 130-132	C137	0.28	2.12	0.43	52.77	0.13	BDL	55.73	0.45	3.44	0.90	94.18	0.19	99.15
1028A-15X-6	Pc. 2, 130-132	C138	0.60	2.24	0.79	52.23	BDL	BDL	55.86	0.97	3.63	1.65	93.22	0.00	99.47
1028A-15X-6	Pc. 2, 130-132	C141	BDL	BDL	BDL	56.49	BDL	BDL	56.54	0.00	0.00	0.00	100.82	0.00	100.82
1028A-15X-6	Pc. 2, 130-132	C144	1.20	3.81	2.59	47.61	BDL	BDL	55.21	1.94	6.17	5.41	84.97	0.00	98.49
1028A-15X-6	Pc. 2, 130-132	C147	1.10	3.16	1.82	49.08	BDL	BDL	55.16	1.77	5.12	3.80	87.60	0.00	98.29
1028A-15X-6	Pc. 2, 130-132	C149	1.09	3.19	1.84	49.81	BDL	BDL	55.93	1.76	5.17	3.84	88.90	0.00	99.67
1028A-15X-6	Pc. 2, 130-132	C150	0.27	0.99	0.32	55.23	BDL	BDL	56.81	0.44	1.60	0.67	98.57	0.00	101.28
1028A-15X-7	Pc. 2, 15-18	C158	BDL	BDL	BDL	56.43	0.40	BDL	56.90	0.00	0.00	0.00	100.72	0.57	101.29
1028A-15X-7	Pc. 2, 15-18	C159	0.18	BDL	BDL	56.73	0.22	BDL	57.13	0.29	0.00	0.00	101.25	0.31	101.85
1028A-15X-7	Pc. 2, 15-18	C160	0.23	1.44	0.22	54.00	BDL	BDL	55.89	0.37	2.33	0.46	96.38	0.00	99.54
1032A-12R-1	Pc. 1, 16-19	C101	0.59	0.57	3.81	49.96	0.11	BDL	55.04	0.95	0.92	7.95	89.17	0.16	99.15
1032A-12R-1	Pc. 1, 16-19	C163	0.79	11.15	2.79	40.91	BDL	BDL	55.64	1.27	18.07	5.82	73.02	0.00	98.18
1032A-12R-1	Pc. 1, 16-19	C164	0.42	7.30	1.57	47.01	BDL	BDL	56.35	0.68	11.83	3.28	83.90	0.07	99.76
1032A-12R-1	Pc. 1, 16-19	C165	0.35	5.63	0.96	48.43	BDL	BDL	55.41	0.56	9.12	2.00	86.44	0.00	98.13
1032A-12R-1	Pc. 1, 16-19	C166	BDL	BDL	BDL	55.77	0.17	BDL	55.94	0.00	0.00	0.00	99.54	0.24	99.78
1032A-13R-2	Pc. 17, 136-143	C175	0.76	0.76	3.07	50.32	1.31	BDL	56.22	1.23	1.23	6.41	89.81	1.87	100.54
1032A-13R-2	Pc. 17, 136-143	C176	BDL	BDL	BDL	54.00	1.25	BDL	55.25	0.00	0.00	0.00	96.38	1.78	98.16
1032A-13R-2	Pc. 17, 136-143	C177	0.26	1.04	2.33	51.90	1.45	BDL	56.98	0.42	1.69	4.86	92.63	2.07	101.66
1032A-13R-2	Pc. 17, 136-143	C180	BDL	BDL	BDL	56.15	BDL	BDL	56.35	0.00	0.00	0.00	100.22	0.00	100.22
1032A-13R-2	Pc. 17, 136-143	C181	BDL	0.32	BDL	54.94	BDL	BDL	55.35	0.00	0.52	0.00	98.06	0.00	98.57
1032A-14R-1	Pc. 10, 39-46	C119	0.47	3.60	1.00	52.14	BDL	BDL	57.25	0.76	5.83	2.09	93.06	0.00	101.74
1032A-14R-1	Pc. 10, 39-46	C213	BDL	0.66	BDL	55.11	BDL	BDL	55.96	0.00	1.07	0.00	98.36	0.00	99.43
1032A-14R-1	Pc. 10, 39-46	C214	0.21	2.86	0.11	52.73	BDL	BDL	55.91	0.34	4.63	0.23	94.11	0.00	99.31
1032A-14R-1	Pc. 10, 39-46	C215	0.24	4.90	1.15	49.21	BDL	BDL	55.55	0.39	7.94	2.40	87.83	0.00	98.56
1032A-14R-1	Pc. 10, 39-46	C216	0.23	0.69	BDL	54.89	BDL	BDL	55.84	0.37	1.12	0.00	97.97	0.00	99.46
1032A-14R-1	Pc. 16A, 89-92	C124	BDL	0.72	BDL	54.41	BDL	BDL	55.35	0.00	1.17	0.00	97.11	0.00	98.28
1032A-14R-1	Pc. 16A, 89-92	C125	BDL	0.37	BDL	54.57	BDL	BDL	55.02	0.00	0.60	0.00	97.40	0.00	98.00
1032A-14R-1	Pc. 16A, 89-92	C127	0.36	0.31	0.19	54.72	BDL	BDL	55.64	0.58	0.50	0.40	97.66	0.00	99.14
1032A-14R-1	Pc. 16A, 89-92	C131	0.27	0.51	0.14	54.92	BDL	BDL	55.84	0.44	0.83	0.29	98.02	0.00	99.57
1032A-14R-1	Pc. 16A, 89-92	C186	0.17	0.51	BDL	55.60	BDL	BDL	56.30	0.27	0.83	0.00	99.23	0.00	100.33
1032A-14R-1	Pc. 16A, 89-92	C190	BDL	0.53	BDL	54.44	BDL	BDL	55.02	0.00	0.86	0.00	97.16	0.00	98.02
1032A-14R-1	Pc. 16A, 89-92	C191	BDL	0.80	BDL	54.56	BDL	BDL	55.51	0.00	1.30	0.00	97.38	0.00	98.67
1032A-14R-1	Pc. 16A, 89-92	C192	BDL	BDL	0.99	53.83	BDL	BDL	54.94	0.00	0.00	2.07	96.07	0.00	98.14
1032A-15R-2	Pc. 8, 63-66	C204	0.16	0.24	BDL	55.53	BDL	BDL	55.96	0.26	0.39	0.00	99.11	0.00	99.76
1032A-15R-2	Pc. 8, 63-66	C208	BDL	BDL	BDL	55.27	BDL	BDL	55.53	0.00	0.00	0.00	98.64	0.00	98.64
1032A-15R-2	Pc. 8, 63-66	C210	BDL	0.31	BDL	55.12	BDL	BDL	55.49	0.00	0.50	0.00	98.38	0.00	98.88
1032A-15R-2	Pc. 8, 63-66	C211	BDL	BDL	BDL	56.12	BDL	BDL	56.27	0.00	0.00	0.00	100.16	0.00	100.16

Notes: All values are in weight percent. BDL = below detection limit. Anl. # = electron microprobe analysis identification number.

namic or kinetic reasons. At the third HT site (Site 1025), carbonate alteration is present in the deeper massive basalts yet absent from the overlying pillow basalts. The warmer temperature of this site (38°C) and more modified basement-water chemistry may combine to allow secondary carbonates to form within the more massive and perhaps less permeable lithology.

Carbonate alteration in the Leg 168 volcanic rocks is very similar to that from 6 Ma volcanic rocks from the Costa Rica Rift. There, similar veins and vesicle fills were sampled from Hole 504B during Deep Sea Drilling Project (DSDP) Legs 69 and 70, and Hole 896A during ODP Leg 148. Tartarotti et al. (1996) described the Hole 896A examples and interpreted most veins as having formed initially as cross-fiber veins during extensional strain. More blocky veins represented either open space filling or replacement of original aragonite fibers by more stable calcite. Calcium carbonates from the Leg 168 transect were described by Hunter (1998) as having formed in two stages, the first being pure $CaCO_3$ and the next having variable compositions with $MgCO_3$, $MnCO_3$, and $FeCO_3$. The present study indicates that the first stage recognized by Hunter (1998) is an aragonite-forming stage, followed by a calcite-forming stage as the basement fluids or physical conditions evolve to allow either direct precipitation of calcite or replacement of aragonite.

One major control on trace and minor elements in either calcite or aragonite is crystallochemical (Deer et al., 1992). The calcite structure accommodates Ca^{2+} (ionic radius 1.00 Å) as well as minor and trace elements having an ionic radius less than or equal to 1.00 Å. The aragonite structure accommodates Ca^{2+} together with minor and trace elements having radii greater that 1.00 Å (Deer et al., 1992). This pattern is followed generally by the Leg 168 carbonates with several exceptions (Table 3). Magnesium, Ni, Cu, and Zn are all elements with small ionic radii, and they are present at higher concentrations in calcite than in aragonite (Mg is 900–3300 ppm in calcite, below detec-

Table 2. Representative electron microprobe analyses of aragonite.

Hole, core, section	Piece, interval (cm)	Anl. #	FeO	MnO	MgO	CaO	SrO	Na_2O	Total	$FeCO_3$	$MnCO_3$	$MgCO_3$	$CaCO_3$	$SrCO_3$	Total
1027C-1R-6	Pc. 2, 65-69	C43	BDL	BDL	BDL	56.12	0.77	BDL	56.89	0.00	0.00	0.00	100.16	1.10	101.26
1027C-1R-6	Pc. 2, 65-69	C44	BDL	BDL	BDL	56.15	0.52	BDL	56.67	0.00	0.00	0.00	100.22	0.74	100.96
1027C-1R-6	Pc. 2, 65-69	C46	BDL	BDL	BDL	56.31	0.22	BDL	56.71	0.00	0.00	0.00	100.50	0.31	100.81
1027C-5R-4	Pc. 9, 127-130	C22	BDL	BDL	BDL	55.28	0.38	0.07	55.73	0.00	0.00	0.00	98.66	0.54	99.20
1027C-5R-4	Pc. 9, 127-130	C24	BDL	BDL	BDL	54.39	1.03	BDL	55.42	0.00	0.00	0.00	97.07	1.47	98.54
1027C-5R-4	Pc. 9, 127-130	C25	BDL	BDL	BDL	54.01	1.05	BDL	55.15	0.00	0.00	0.00	96.40	1.50	97.89
1027C-5R-4	Pc. 9, 127-130	C26	BDL	BDL	BDL	54.55	0.52	BDL	55.10	0.00	0.00	0.00	97.36	0.74	98.10
1027C-5R-4	Pc. 9, 127-130	C27	BDL	BDL	BDL	55.32	0.21	BDL	55.53	0.00	0.00	0.00	98.73	0.30	99.03
1027C-5R-4	Pc. 9, 127-130	C28	BDL	BDL	BDL	55.92	0.19	BDL	56.11	0.00	0.00	0.00	99.81	0.27	100.08
1027C-5R-4	Pc. 9, 127-130	C29	BDL	BDL	BDL	55.00	0.44	0.08	55.57	0.00	0.00	0.00	98.16	0.63	98.79
1027C-5R-4	Pc. 9, 127-130	C30	BDL	BDL	BDL	54.86	0.28	BDL	55.26	0.00	0.00	0.00	97.91	0.40	98.31
1027C-5R-6	Pc. 6, 40-49	C57	BDL	BDL	BDL	56.56	0.32	BDL	56.97	0.00	0.00	0.00	100.95	0.46	101.40
1027C-5R-6	Pc. 6, 40-49	C58	BDL	BDL	BDL	55.49	0.37	BDL	55.88	0.00	0.00	0.00	99.04	0.53	99.56
1027C-5R-6	Pc. 6, 40-49	C60	BDL	BDL	BDL	54.69	0.37	BDL	55.26	0.00	0.00	0.00	97.61	0.53	98.14
1027C-5R-6	Pc. 6, 40-49	C62	BDL	BDL	BDL	55.91	0.11	BDL	56.02	0.00	0.00	0.00	99.79	0.16	99.94
1027C-5R-6	Pc. 6, 40-49	C65	BDL	BDL	BDL	56.85	0.13	0.08	57.06	0.00	0.00	0.00	101.46	0.19	101.65
1028A-15X-6	Pc. 2, 130-132	C72	BDL	BDL	BDL	55.46	0.16	BDL	55.66	0.00	0.00	0.00	98.98	0.23	99.21
1028A-15X-6	Pc. 2, 130-132	C84	BDL	BDL	BDL	55.27	0.19	0.08	55.65	0.00	0.00	0.00	98.64	0.27	98.92
1032A-12R-1	Pc. 1, 16-19	C162	BDL	BDL	BDL	55.96	0.53	BDL	56.53	0.00	0.00	0.00	99.88	0.76	100.63
1032A-12R-1	Pc. 1, 16-19	C167	BDL	BDL	BDL	56.23	0.21	BDL	56.44	0.00	0.00	0.00	100.36	0.30	100.66
1032A-12R-3	Pc. 7, 32-35	C103	BDL	BDL	BDL	53.38	1.82	0.12	55.41	0.00	0.00	0.00	95.27	2.59	97.86
1032A-12R-3	Pc. 7, 32-35	C106	BDL	BDL	BDL	53.28	2.16	0.08	55.65	0.00	0.00	0.00	95.09	3.08	98.17
1032A-12R-3	Pc. 7, 32-35	C168	BDL	BDL	BDL	56.23	0.54	BDL	56.82	0.00	0.00	0.00	100.36	0.77	101.13
1032A-12R-3	Pc. 7, 32-35	C169	BDL	BDL	BDL	55.62	0.69	BDL	56.33	0.00	0.00	0.00	99.27	0.98	100.25
1032A-12R-3	Pc. 7, 32-35	C170	BDL	BDL	BDL	56.49	0.50	BDL	57.06	0.00	0.00	0.00	100.82	0.71	101.53
1032A-12R-3	Pc. 7, 32-35	C172	BDL	BDL	BDL	56.42	0.73	BDL	57.25	0.00	0.00	0.00	100.70	1.04	101.74
1032A-12R-3	Pc. 7, 32-35	C173	BDL	BDL	BDL	55.82	0.42	BDL	56.24	0.00	0.00	0.00	99.63	0.60	100.22
1032A-12R-3	Pc. 7, 32-35	C174	BDL	BDL	BDL	55.68	0.86	BDL	56.63	0.00	0.00	0.00	99.38	1.23	100.60
1032A-13R-2	Pc. 17, 136-143	C178	BDL	BDL	BDL	56.55	0.24	BDL	56.86	0.00	0.00	0.00	100.93	0.34	101.27
1032A-13R-2	Pc. 17, 136-143	C182	BDL	BDL	BDL	54.92	1.11	BDL	56.03	0.00	0.00	0.00	98.02	1.58	99.60
1032A-14R-1	Pc. 16A, 89-92	C129	BDL	0.94	BDL	55.16	0.32	BDL	56.42	0.00	1.52	0.00	98.45	0.46	100.43
1032A-14R-1	Pc. 10, 39-46	C217	BDL	0.31	BDL	55.67	0.19	BDL	56.17	0.00	0.50	0.00	99.36	0.27	100.13
1032A-15R-1	Pc. 16, 81-84	C194	BDL	BDL	BDL	55.77	0.35	BDL	56.12	0.00	0.00	0.00	99.54	0.50	100.04
1032A-15R-1	Pc. 16, 81-84	C195	BDL	BDL	BDL	56.09	0.58	BDL	56.72	0.00	0.00	0.00	100.11	0.83	100.93
1032A-15R-1	Pc. 16, 81-84	C196	BDL	BDL	BDL	56.20	0.56	BDL	56.83	0.00	0.00	0.00	100.30	0.80	101.10
1032A-15R-1	Pc. 16, 81-84	C197	BDL	BDL	BDL	56.12	0.13	BDL	56.27	0.00	0.00	0.00	100.16	0.19	100.35
1032A-15R-1	Pc. 16, 81-84	C198	BDL	BDL	BDL	56.37	0.58	BDL	56.95	0.00	0.00	0.00	100.61	0.83	101.43
1032A-15R-1	Pc. 16, 81-84	C199	BDL	BDL	BDL	56.15	0.21	BDL	56.40	0.00	0.00	0.00	100.22	0.30	100.51
1032A-15R-1	Pc. 16, 81-84	C201	BDL	BDL	BDL	56.96	0.14	BDL	57.12	0.00	0.00	0.00	101.66	0.20	101.86
1032A-15R-2	Pc. 8, 63-66	C202	BDL	BDL	BDL	56.98	0.12	BDL	57.15	0.00	0.00	0.00	101.70	0.17	101.87
1032A-15R-2	Pc. 8, 63-66	C205	BDL	BDL	BDL	56.79	0.20	BDL	57.09	0.00	0.00	0.00	101.36	0.29	101.64
1032A-15R-2	Pc. 8, 63-66	C209	BDL	BDL	BDL	56.12	0.40	BDL	56.61	0.00	0.00	0.00	100.16	0.57	100.73

Notes: All values are in weight percent. BDL = below detection limit. Anl. # = electron microprobe analysis identification number.

tion limit [BDL] to 150 ppm in aragonite; Ni is 800–1300 ppm in calcite and 100–410 ppm in aragonite; Cu is 400–1100 ppm in calcite and BDL–50 ppm in aragonite; and Zn is 1100–2100 ppm in calcite and 100–300 ppm in aragonite). Similarly, Rb and Sr are large-ionic-radius elements that are concentrated in aragonite (Rb is BDL–2 ppm in calcite and 20–50 ppm in aragonite; and Sr is 100–600 ppm in calcite and 3700–7700 ppm in aragonite). The exceptions are La, Ce, and Pb, which have large ionic radii, yet are present at higher concentrations in calcites than aragonites (La is BDL–200 ppm in calcite and BDL in aragonite; Ce is 20–200 ppm in calcite and BDL in aragonite; and Pb is BDL–1200 ppm in calcite and BDL–160 ppm in aragonite).

The minor and trace element concentrations in carbonate vein minerals, combined with knowledge of the relevant equilibrium distribution coefficients (K_ds) between solution and carbonate mineral, make it possible to predict certain chemical characteristics of the hydrothermal fluids responsible for the veining. Rimstidt et al. (1998) provide estimated K_ds as a function of temperature for calcite, and Hart et al. (1994) adopted a K_d for Sr in aragonite. Table 4 presents results utilizing these K_ds, giving the predicted equilibrium fluid parameters based on analyses of two calcites and two aragonites.

Two elements, Mg and Sr, are significantly depleted in the estimated calcite-forming hydrothermal fluid relative to seawater. The estimated Ca/Mg values are 20–30 times the seawater value, reflecting the fact that the hydrothermal fluid has lost much of its Mg to basalt–seawater interaction, consistent with numerous fluid-chemistry studies (e.g., Mottl et al., 1998; Davis, Fisher, Firth, et al., 1997).

The estimated Ca/Sr values based on the two aragonite samples (48–71) are indistinguishable from the seawater value of Ca/Sr = 51. However, the estimated Ca/Sr values based on the two calcite samples (116–193) are roughly 2–4 times the seawater Ca/Sr value (51). This suggests that although aragonite may have formed from a solution barely modified from seawater in its Sr concentration, the calcite formed from a modified fluid, consistent with the notion that low-temperature seawater–basalt interaction results in a lowering of the fluid Sr (Burns et al., 1992; Hart et al., 1994). However, because extensive water–rock reaction should result in a very high Ca/Sr, exceeding several thousand (Hart et al., 1994), the calcite-forming fluid estimated in Table 4 has only just begun to become modified from the original seawater Sr concentration.

In contrast to Mg and Sr, which are depleted, the minor and trace element data indicate that the estimated hydrothermal solutions during the calcite growth are very much enriched in Fe, Mn, Co, Ni, Cu, and Zn (Table 4). The Ca/Co, Ca/Cu, Ca/Zn, and Ca/Fe values are all reduced by about one order of magnitude relative to seawater, and the Ca/Ni and Ca/Mn values are reduced about three orders of magnitude. This shows that Co, Cu, Zn, and Fe are all enriched to about the same degree in the hydrothermal solution, whereas Ni and Mn exhibit enrichments about 100 times higher. Perhaps related to this is the observation by Porter et al. (Chap. 12, this volume) that a clay vein from Site 1026 contains saponite whose trace element characteristics include an unusually high Ni concentration, presumably derived from alteration of particularly Ni-rich olivine in the host basalt.

Secondary calcium carbonates are sinks for minor and trace elements in subseafloor hydrothermal systems. Depending on the amount of carbonate alteration present, aragonite could be a minor sink for Zn, Rb, and, especially, for Sr (Tables 2, 3). Calcite could be a very minor sink for Sr, La, and Ce and a more significant sink for Mg, Mn, Ni, Cu, Zn, and Pb (Tables 1, 3). Replacement of aragonite

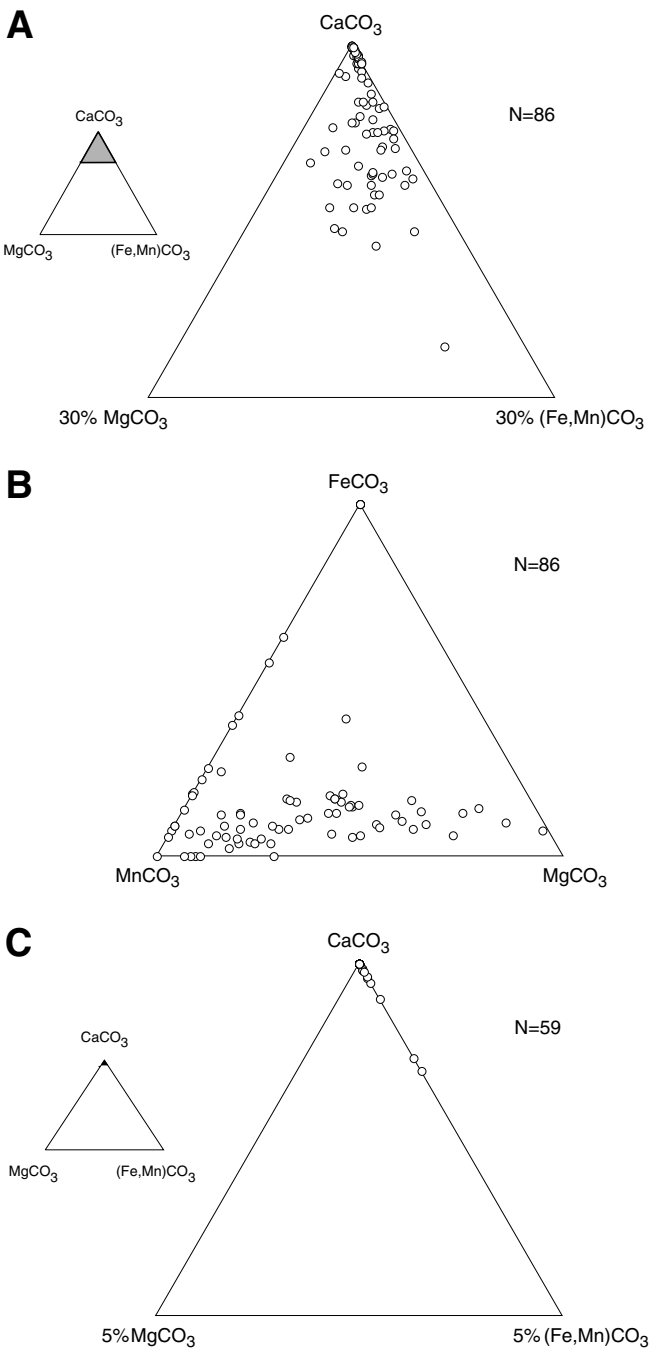

Figure 2. Electron microprobe analyses of carbonate minerals. **A.** Relative contributions (wt%) of $CaCO_3$, $MgCO_3$, and (Fe + Mn)CO_3 to the overall mineral analysis for calcite. Eighty-six analyses are plotted. The inset shows the range of compositions represented by the diagram. **B.** Relative contribution (wt%) of minor components $FeCO_3$, $MnCO_3$, and $MgCO_3$ to the chemical composition of calcite ($CaCO_3$). **C.** Relative contributions (wt%) of $CaCO_3$, $MgCO_3$, and (Fe + Mn)CO_3 to the overall mineral analysis for aragonite. Fifty-nine analyses are plotted. The inset shows the range of compositions represented by the diagram. Note that this range is smaller than that of Part A.

by calcite is a process that tends to release Sr, Rb, and Zn to solution and to partially remove Mg, Mn, Ni, Cu, Zn, and Pb from solution.

CONCLUSIONS

1. Calcium carbonate occurs in 0.5- to 2-mm-wide veins within many basement rocks from the Leg 168 transect. Crosscutting relationships indicate that the carbonate minerals generally occur late in the alteration sequence. The temperatures of present-day water–rock interaction at sites with evidence of carbonate mineralization range from 38° to 64°C.

2. Calcium carbonate textures vary widely, with calcite-aragonite intergrowths, monomineralic veins, and compositionally zoned minerals common.

3. Calcite and aragonite analyses exhibit systematic differences: calcite contains appreciable $MgCO_3$, $MnCO_3$, and $FeCO_3$, whereas aragonite contains essentially no $MgCO_3$ and very little $MnCO_3$ or $FeCO_3$. Furthermore, calcite contains more Ni, Cu, Zn, La, Ce, and Pb relative to aragonite, and aragonite contains more Sr and Rb relative to calcite.

4. Fluid inclusions in aragonite suggest trapping temperatures well below 100°C and ice melting temperatures consistent with the expected freezing-point depression of seawater, confirming that the aragonite most likely precipitated at low temperature from a seawater-derived basement fluid of normal seawater salinity.

5. Trace element analyses combined with available distribution coefficients suggest that the solution from which calcite precipitated was significantly depleted in Mg and Sr relative to seawater, whereas it was significantly enriched in Fe, Mn, Co, Ni, Cu, and Zn. Aragonite, on the other hand, precipitated from a solution that was not particularly distinct from seawater, at least in its Sr concentration.

ACKNOWLEDGMENTS

We wish to thank the Master and crew of *JOIDES Resolution* for Leg 168, the Ocean Drilling Program personnel, and the other members of the shipboard scientific party, all of whom worked together to make Leg 168 a success. Chris Fleisher assisted in electron microprobe analysis at the University of Georgia, and Michelle Shearer and Buffie Chournos assisted in sample preparation for thin sectioning and LA–ICP-MS analysis. James Brewer collected fluid inclusion ice melting measurements. This study was supported through a JOI/USSAC grant as well as ICP-MS support from the National Science Foundation (EAR-9405716 and EAR-950623). Helpful comments about this paper were graciously provided by Damon Teagle, Carlota Escutia, and an anonymous reviewer.

REFERENCES

Alt, J.C., Honnorez, J., Laverne, C., and Emmermann, R., 1986. Hydrothermal alteration of a 1 km section through the upper oceanic crust, Deep Sea Drilling Project Hole 504B: mineralogy, chemistry, and evolution of seawater-basalt interactions. *J. Geophys. Res.,* 91:10309–10335.

Anderson, R.N., Langseth, M.G., and Sclater, J.G., 1977. The mechanisms of heat transfer through the floor of the Indian Ocean. *J. Geophys. Res.,* 82:3391–3409.

Burns, S.J., Baker, P.A., and Elderfield, H., 1992. Timing of carbonate mineral precipitation and fluid flow in sea-floor basalts, northwest Indian Ocean. *Geology,* 20:255–258.

Davis, E.E., Chapman, D.S., Mottl, M.J., Bentkowski, W.J., Dadey, K., Forster, C., Harris, R., Nagihara, S., Rohr, K., Wheat, G., and Whiticar, M.,

1992. FlankFlux: an experiment to study the nature of hydrothermal circulation in young oceanic crust. *Can. J. Earth Sci.,* 29:925–952.
Davis, E.E., and Currie, R.G., 1993. Geophysical observations of the northern Juan de Fuca Ridge system: lessons in sea-floor spreading. *Can. J. Earth Sci.,* 30:278–300.
Davis, E.E., Fisher, A.T., Firth, J.V., et al., 1997. *Proc. ODP, Init. Repts.,* 168: College Station, TX (Ocean Drilling Program).
Deer, W.A., Howie, R.A., and Zussman, J., 1992. *An Introduction to the Rock-Forming Minerals:* Harlow (Longman).
Drever, J.I., 1982. *The Geochemistry of Natural Waters:* London (Prentice-Hall).
Goldstein, R.H., and Reynolds, T.J., 1994. *Systematics of Fluid Inclusions in Diagenetic Minerals.* SEPM Short Course 31: Tulsa, OK (Soc. Econ. Paleontol. Mineral.).
Hart, S.R., Blusztajn, J., Dick, H.J.B., and Lawrence, J.R., 1994. Fluid circulation in the oceanic crust: contrast between volcanic and plutonic regimes. *J. Geophys. Res.,* 99:3163–3174.
Hart, S.R., and Staudigel, H., 1986. Ocean crust vein mineral deposition: Rb/Sr ages, U-Th-Pb geochemistry, and duration of circulation at DSDP Sites 261, 462 and 516. *Geochim. Cosmochim. Acta,* 50:2751–2761.
Hunter, A.G., 1998. Petrological investigations of low temperature hydrothermal alteration of the upper crust, Juan de Fuca Ridge, ODP Leg 168. *Geol. Soc. Spec. Publ. London,* 148:99–125.
Jenner, G.A., Foley, S.F., Jackson, S.E., Green, H., Fryer, B.J., and Longerich, H.P., 1993. Determination of partition coefficients for trace elements in high pressure-temperature experimental run products by laser ablation microprobe-inductively coupled plasma-mass spectrometry (LAM-ICP-MS). *Geochim. Cosmochim. Acta,* 58:5099–5103.
Johnson, H.P., and Holmes, M.L., 1989. Evolution in plate tectonics: a study of the Juan de Fuca Ridge. *In* Winterer, E.L., Hussong, D.M., and Decker, R.E. (Eds.), *The Eastern Pacific Ocean and Hawaii.* Geol. Soc. Am., Geol. of North Am. Ser., N:73–91.
Kontak, D.J., and Jackson, S., 1995. Laser-ablation ICP-MS micro-analysis of calcite cement from a Mississippi-valley-type Zn-Pb deposit, Nova Scotia: dramatic variability in REE content on macro- and micro-scales. *Can. Mineral.,* 33:445–467.
Marshall, D.J., 1988. *Cathodoluminescence of Geological Materials:* Boston (Unwin Hyman).
Mottl, M.J., and Wheat, C.G., 1994. Hydrothermal circulation through mid-ocean ridge flanks: fluxes of heat and magnesium. *Geochim. Cosmochim. Acta,* 58:2225–2238.
Mottl, M.J., Wheat, C.G., Baker, E., Becker, N., Davis, E., Feely, R., Grehan, A., Kadko, D., Lilley, M., Massoth, G., Moyer, C., and Sansone, F., 1998. Warm springs discovered on 3.5 Ma oceanic crust, eastern flank of the Juan de Fuca Ridge. *Geology,* 26:51–54.
Perkins, W.T., and Pearce, N.J.G., 1995. Mineral microanalysis by laserprobe inductively coupled plasma mass spectrometry. *In* Potts, P.J., Bowles, J.F.W., Reed, S.J.B., and Cave, M.R. (Eds.), *Microprobe Techniques in the Earth Sciences:* London (Chapman and Hall), 291–325.
Purdy, G.M., 1987. New observations of the shallow seismic structure of young oceanic crust. *J. Geophys. Res.,* 92:9351–9362.
Ramsay, J.G., 1980. The crack-seal mechanism of rock deformation. *Nature,* 284:135–139.
Rimstidt, J.D., Balog, A., and Webb, J., 1998. Distribution of trace elements between carbonate minerals and aqueous solutions. *Geochim. Cosmochim. Acta,* 62:1851–1863.
Sclater, J.G., Crowe, J., and Anderson, R.N., 1976. On the reliability of ocean heat flow averages. *J. Geophys. Res.,* 81:2997–3006.
Stein, C.A., and Stein, S., 1994. Constraints on hydrothermal heat flux through the oceanic lithosphere from global heat flow. *J. Geophys. Res.,* 99:3081–3095.
Tartarotti, P., Vanko, D.A., Harper, G.D., and Dilek, Y., 1996. Crack-seal veins in upper Layer 2 in Hole 896A. *In* Alt, J.C., Kinoshita, H., Stokking, L.B., and Michael, P.J. (Eds.), *Proc. ODP, Sci. Results,* 148: College Station, TX (Ocean Drilling Program), 281–288.

Date of initial receipt: 11 December 1998
Date of acceptance: 4 August 1999
Ms 168SR-003

APPENDIX

Laser ablation ICPMS analytical procedures.

Quantification for LA–ICP-MS was accomplished using the National Institute of Standards and Technology standard reference material 611 (SRM-611), which contains numerous trace elements at about 500 ppm, following the procedures reported by Perkins and Pearce (1995), Kontak and Jackson (1995), and Jenner et al. (1993). Calcium, present in SRM-611 at 12 wt% CaO and determined by electron microprobe in the carbonate samples to be 51 wt% CaO, served as an internal standard to correct for differences in the ablation yields between the SRM-611 glass and the carbonate samples.

The equation for calculating the concentration of an element in the specimen is

$$C_{el}^{spec} = C_{el}^{SRM\text{-}611} \times \frac{(cts_{el}/cts_{Ca})^{spec}}{(cts_{el}/cts_{Ca})^{SRM\text{-}611}} \times \frac{C_{Ca}^{spec}}{C_{Ca}^{SRM\text{-}611}}.$$

The concentrations of each minor element in the SRM-611 reference material are known to about 2 relative % (rel%), as is the concentration of Ca, the internal standard, in the specimen. The ratio of element counts to calcium counts in SRM-611, corrected for the instrument blank, varied with a standard deviation ranging from 10 to 40 rel%, depending on the element. This value is given in the last row of Table 3 as "RSD (element/Ca)rm." Each of the terms, then, contributes a component of error to the estimation of $C_{el}^{spec.}$; however, the final error is not simply the sum of the individual term errors because of the probability that a random high estimate of one term in the numerator will be partly or wholly compensated by a low estimate of another term in the numerator or a high estimate of a denominator term. At this preliminary stage of development of the LA–ICP-MS analytical technique, we think that the RSD for the ratio of element counts and Ca counts (reported in the last row of Table 3) serves as a qualitative estimate of the uncertainty in the calculated results reported in the table.

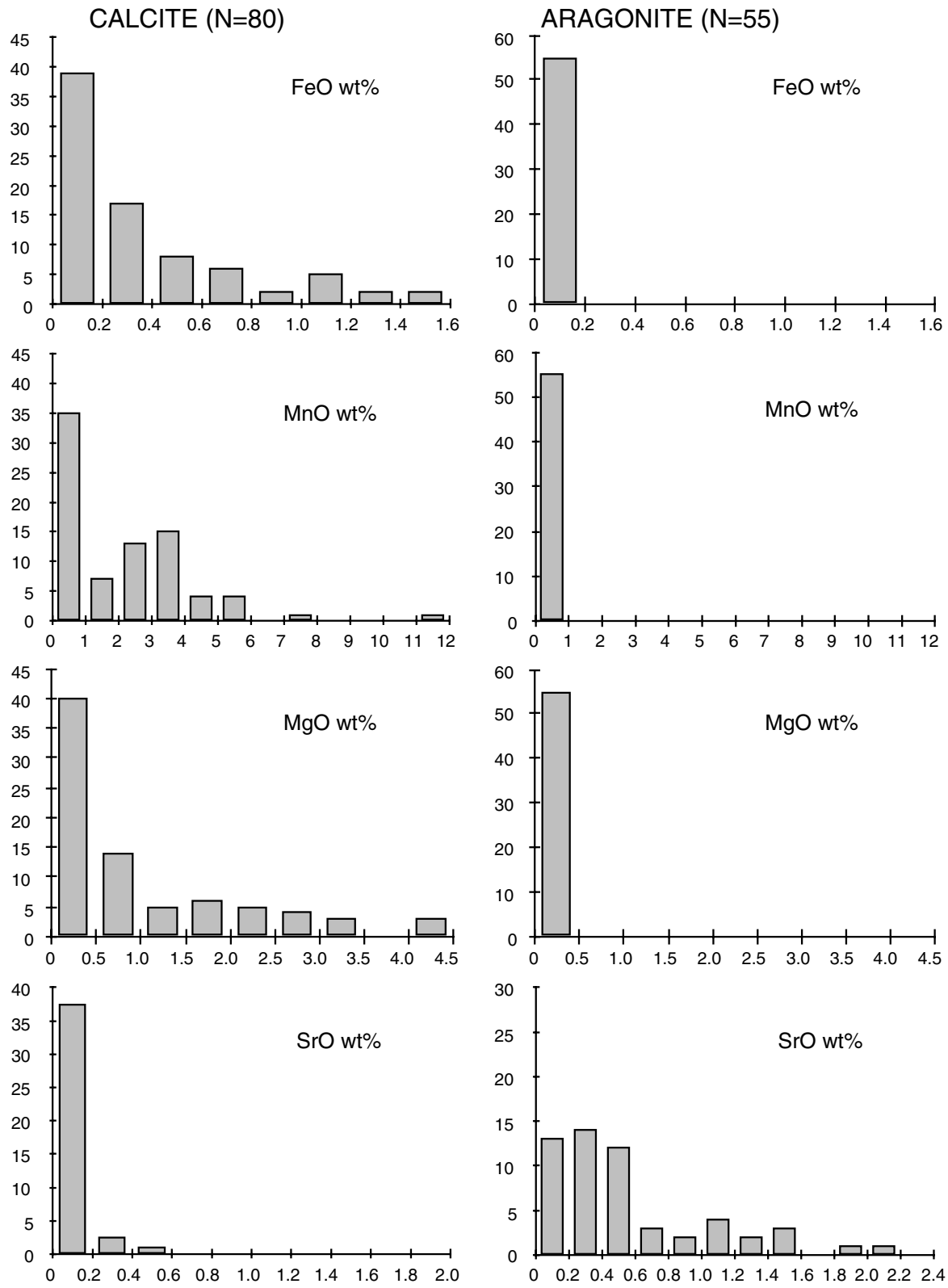

Figure 3. Frequency histograms of the concentrations of minor element oxides in both calcite and aragonite, determined by electron microprobe (N = number of data). Data for calcites are on the left, and data for aragonites are on the right. Calcite contains variable and appreciable amounts of FeO, MnO, and MgO, and only small amounts of SrO, whereas aragonites contain appreciable SrO and very little FeO, MnO, and MgO.

Table 3. Laser-ablation ICP-MS analyses of calcite and aragonite from Leg 168.

Sample #	Mineral	Mg	Co	Ni	Cu	Zn	Rb	Sr	La	Ce	^{206}Pb	^{208}Pb	U
Ionic Radius (A)		0.72	0.65	0.70	0.73	0.74	1.52	1.16	1.06	1.03	1.19	1.19	0.89
Experiment #1													
168-1027B-61X-CC, Pc. 28, 29-30 cm													
Ablation 1	Calcite	2400	BDL	1200	800	1800	BDL	100	70	80	700	600	BDL
Ablation 2	Calcite	2700	BDL	1300	1100	2100	BDL	200	200	100	1200	900	BDL
Ablation 3	Calcite	2300	BDL	900	700	1500	BDL	200	70	200	900	500	BDL
Ablation 4	Calcite	2400	BDL	1100	800	1700	BDL	100	80	40	1000	600	BDL
Ablation 5	Calcite	2100	10	900	800	1600	BDL	200	100	30	1100	500	BDL
Ablation 6	Calcite	2100	5	900	700	1500	BDL	200	100	50	900	400	BDL
Ablation 7	Calcite	2000	10	800	700	1500	BDL	200	100	50	500	400	BDL
168-1032A-14R-1, Pc. 10, 39-46 cm													
Ablation 1	Calcite	1300	BDL	800	500	1100	BDL	400	BDL	20	300	100	BDL
Ablation 2	Calcite	900	BDL	800	500	1100	BDL	100	BDL	60	300	200	BDL
Ablation 3	Calcite	1800	BDL	900	400	1200	BDL	500	40	50	300	200	BDL
Ablation 4	Calcite	1800	BDL	1000	600	1300	BDL	200	30	90	400	200	BDL
Ablation 5	Calcite	3300	10	800	500	1100	BDL	500	20	50	400	200	BDL
Ablation 6	Calcite	2000	BDL	800	500	1300	BDL	600	90	60	200	200	BDL
168-1027C-5R-6, Pc. 6, 47-50 cm													
Ablation 1	Aragonite	100	BDL	140	BDL	200	20	4100	BDL	BDL	BDL	BDL	BDL
Ablation 2	Aragonite	BDL	BDL	100	20	200	30	4000	BDL	BDL	BDL	BDL	BDL
Ablation 3	Aragonite	120	BDL	140	40	200	20	4200	BDL	BDL	BDL	50	BDL
Ablation 5	Aragonite	120	BDL	110	BDL	100	40	5100	BDL	BDL	BDL	20	BDL
Ablation 6	Aragonite	BDL	BDL	120	20	200	30	5700	BDL	BDL	BDL	30	BDL
Ablation 7	Aragonite	140	10	140	BDL	200	20	3700	BDL	BDL	160	BDL	BDL
168-1027C-5R-4, Pc. 9, 127-130 cm													
Ablation 1	Aragonite	BDL	BDL	270	BDL	200	40	6500	BDL	BDL	BDL	BDL	BDL
Ablation 2	Aragonite	150	BDL	410	50	200	40	5900	BDL	BDL	BDL	BDL	BDL
Ablation 3	Aragonite	BDL	BDL	220	BDL	200	30	7300	BDL	BDL	BDL	BDL	BDL
Ablation 4	Aragonite	BDL	BDL	240	BDL	100	50	6500	BDL	BDL	50	BDL	BDL
Ablation 5	Aragonite	BDL	BDL	180	BDL	200	40	6300	BDL	BDL	BDL	BDL	BDL
Ablation 6	Aragonite	BDL	BDL	210	20	100	20	6800	BDL	BDL	BDL	BDL	BDL
Ablation 7	Aragonite	BDL	BDL	140	20	200	30	7700	BDL	BDL	30	20	BDL
Experiment #2													
168-1027C-5R-4, Pc. 9, 127-130 cm													
Ablation 1	Aragonite	80	BDL	300	20	200	30	6500	BDL	BDL	BDL	20	BDL
Ablation 2	Aragonite	140	7	380	30	200	30	7300	BDL	BDL	25	BDL	BDL
Ablation 3	Aragonite	130	BDL	370	30	300	30	6900	BDL	BDL	BDL	BDL	BDL
Statistical data													
SDL (ppm):		2	1	6	1	13	1	1	2	2	13	5	4
MDL (ppm):		11	6	89	10	117	10	5	10	10	23	15	17
RSD (element/Ca)rm, (%):		13	22	11	17	37	23	22	34	40	22	22	47

Notes: All concentrations are in parts per million (ppm). SDL = statistical detection limit, equal to three times the concentration equivalent of the square root of background counts, determined on the SRM-611 glass reference material. MDL = minimum detection limit after Jenner et al. (1993). RSD = relative standard deviation as defined in the Appendix.

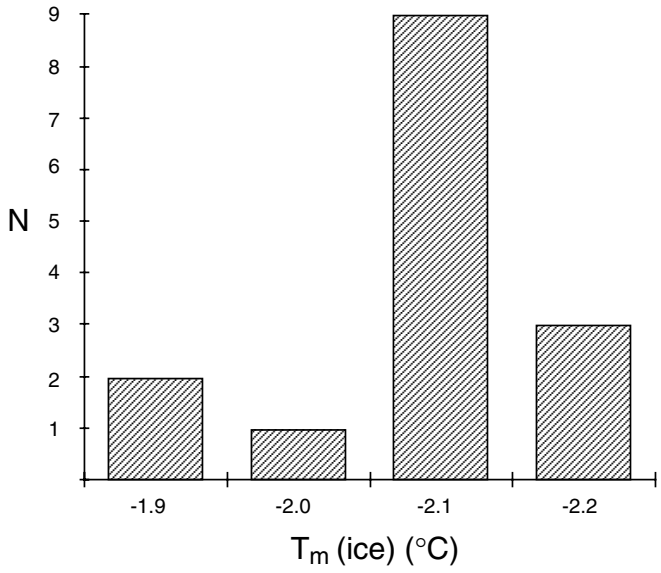

Figure 4. Frequency histogram of ice melting point determinations for fluid inclusions in aragonite from Sample 168-1027C-5R-4, 127–130 cm (Piece 9). These measurements are accurate to ±0.1°C. The ice melting point in normal seawater is –2.1°C.

Table 4. Average hydrothermal fluid parameters calculated from minor and trace element concentrations in carbonate vein minerals.

Hole, core, section, piece, interval (cm)	Mineral	Element	Avg. ppm in mineral	Kd value (@ 60°C)	Ca/element in fluid	Ca/element in seawater
1027B-61X-CC, Pc. 28, 29-30	Calcite	Mg	2,300	0.041	7	0.32
1032A-14R-1, Pc.10, 39-46	Calcite	Mg	1,850	0.041	10	0.32
1027B-61X-CC, Pc. 28, 29-30	Calcite	Co	8	11.21	598,465	8,220,000
1032A-14R-1, Pc.10, 39-46	Calcite	Co	10	11.21	448,848	8,220,000
1027B-61X-CC, Pc. 28, 29-30	Calcite	Ni	1,000	0.41	166	822,000
1032A-14R-1, Pc.10, 39-46	Calcite	Ni	850	0.41	195	822,000
1027B-61X-CC, Pc. 28, 29-30	Calcite	Cu	800	80.2	41,034	822,000
1032A-14R-1, Pc.10, 39-46	Calcite	Cu	500	80.2	65,116	822,000
1027B-61X-CC, Pc. 28, 29-30	Calcite	Zn	1,700	18.5	4,492	205,500
1032A-14R-1, Pc.10, 39-46	Calcite	Zn	1,200	18.5	6,295	205,500
1027B-61X-CC, Pc. 28, 29-30	Calcite	Sr	170	0.075	193	51
1032A-14R-1, Pc.10, 39-46	Calcite	Sr	380	0.075	116	51
1027C-5R-6, Pc. 6, 47-50	Aragonite	Sr	4,500	0.8	71	51
1027C-5R4, Pc. 9, 127-130	Aragonite	Sr	6,800	0.8	48	51
1027B-61X-CC, Pc. 28, 29-30	Calcite	Mn	30,800	14.6	190	2,055,000
1032A-14R-1, Pc.10, 39-46	Calcite	Mn max.	38,000	14.6	154	2,055,000
1032A-14R-1, Pc.10, 39-46	Calcite	Mn min.	5,000	14.6	1,144	2,055,000
1032A-14R-1, Pc.10, 39-46	Calcite	Fe	3,600	25.4	2,784	205,500
1032A-14R-1, Pc.10, 39-46	Calcite	Fe	1,100	25.4	9,346	205,500

Notes: Distribution coefficients (Kd) are for 60°C, from Rimstidt et al. (1998), except the Kd for Sr in aragonite, which is that adopted by Hart et al. (1994). Seawater values are from Drever (1982).

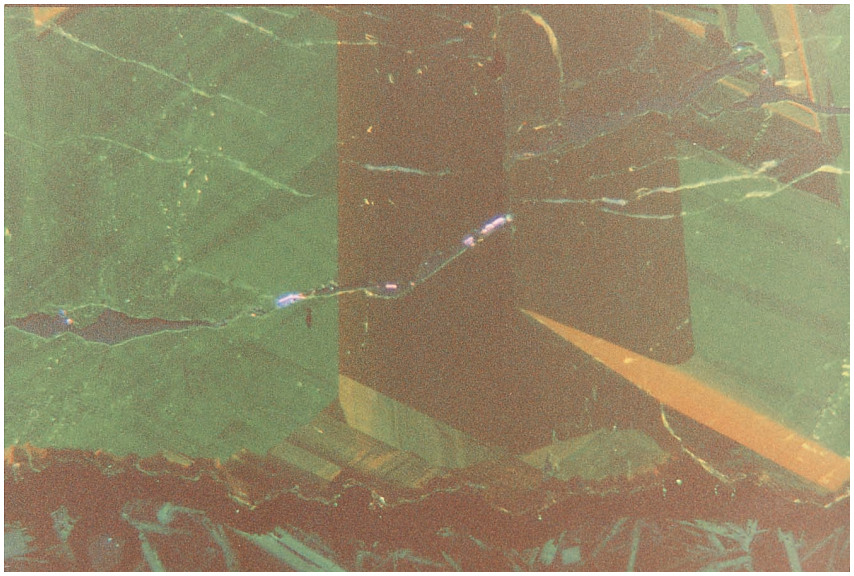

1

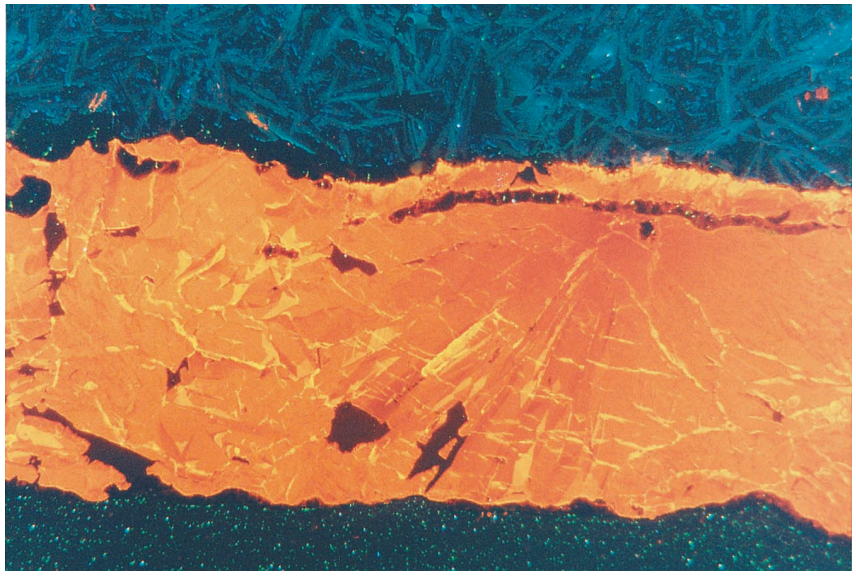

2

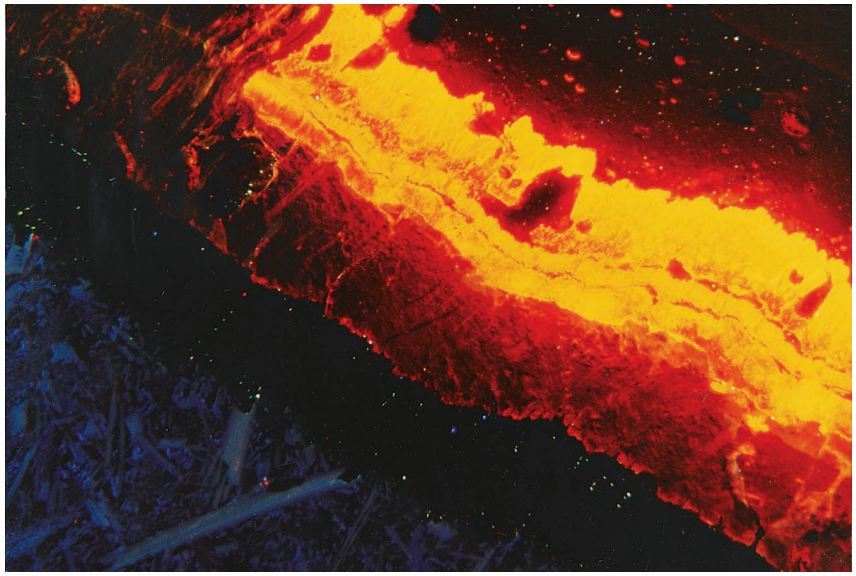

3

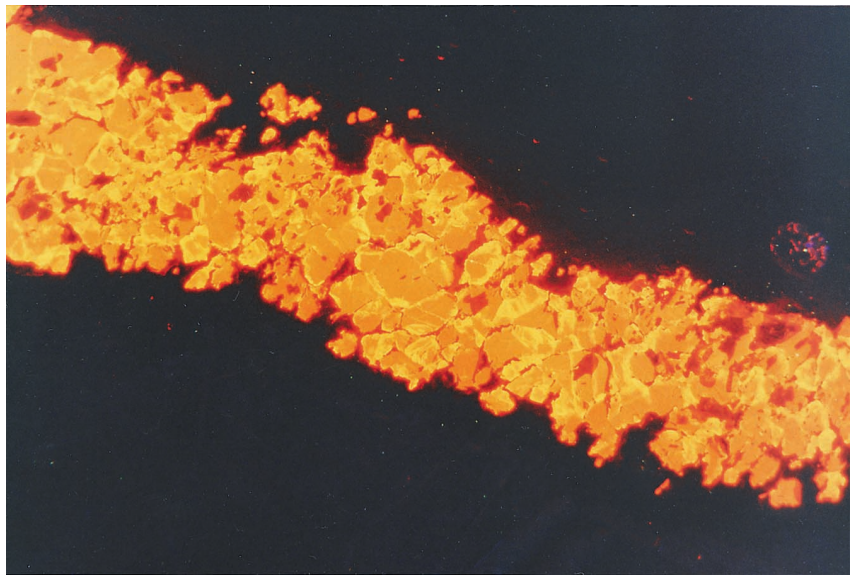

4

Plate 1. Photomicrographs of carbonate veins from Leg 168 basalt specimens, taken using cathodoluminescence (CL). **1.** Blocky aragonite vein with basalt host rock visible along bottom edge. The aragonite is optically clear and homogeneous; however, the CL image reveals complex zones of varying CL color and intensity. Purple luminescence is from polishing compound (alumina?) stuck in epoxy that fills a microcrack through the section. Sample 168-1027C-5R-4, Piece 9. **2.** Blocky and radial-fibrous calcite vein with basalt host visible along top. Although relatively homogeneous, bright areas may indicate zones of variable trace element concentrations. Sample 168-1027B-61X-CC, Piece 28. **3.** Zoned vein with cross-fiber calcite in the middle (bright CL) and blocky aragonite (dark CL) at the edge. Host rock is visible at lower left. Sample 168-1032A-12R-1, Piece 1. **4.** Blocky and granular calcite vein with zoned CL intensity. The outside edge of most calcite crystals have brighter CL, indicating more luminescence activators in the zone. Sample 168-1032A-12R-1, Piece 1.

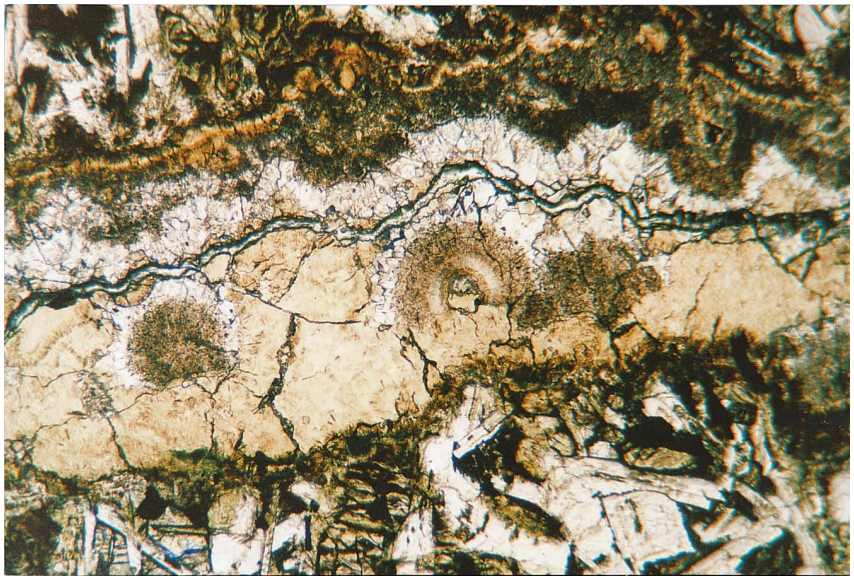

1

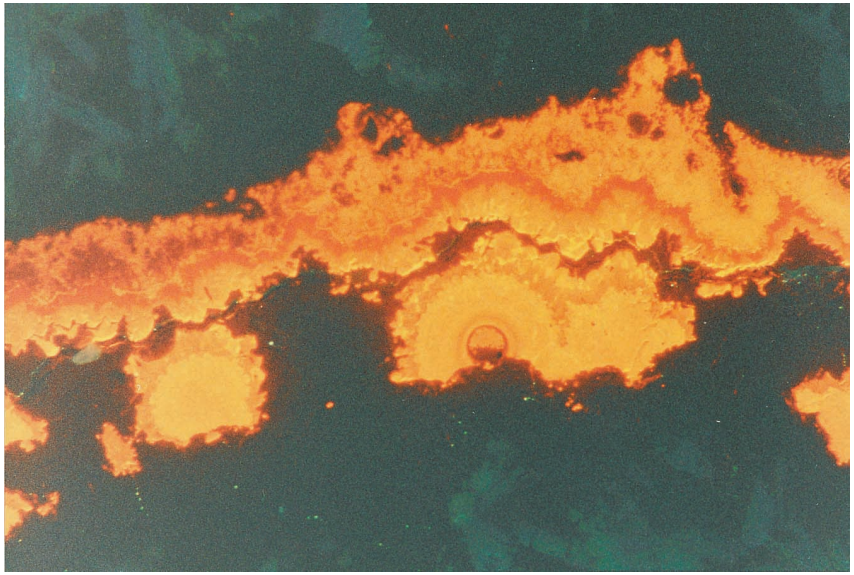

2

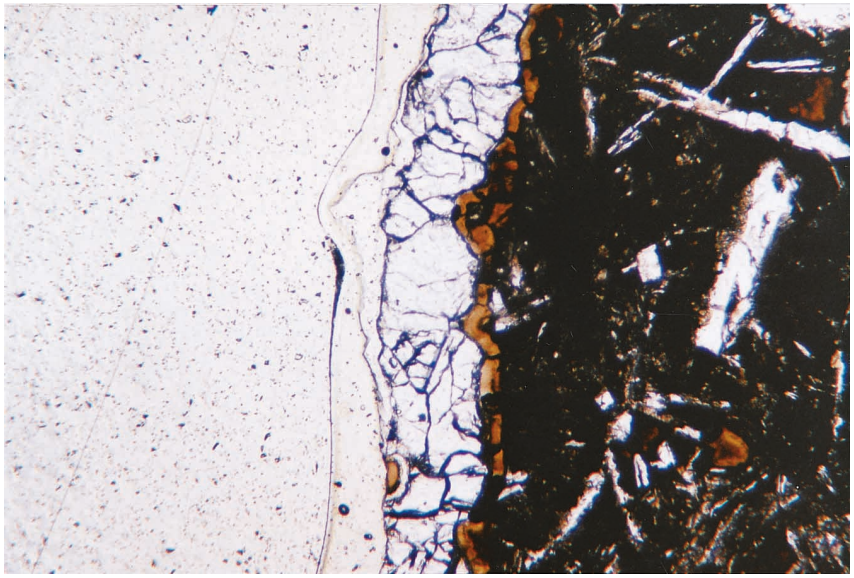

3

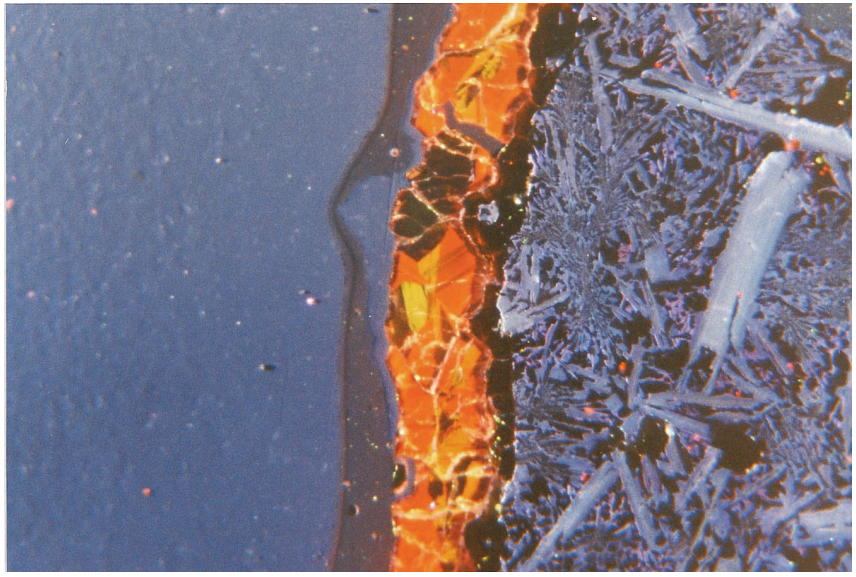

4

Plate 2. Photomicrographs of carbonate veins from Leg 168 basalt specimens, taken using cathodoluminescence (CL). **1.** Plane-light photograph of a complex vein filled with fibrous clay at the margins (brown, fuzzy), followed by light tan clay (tan), spherulitic calcite (brown spherules), and blocky calcite (clear). The medial crack is filled with epoxy. Host rock is visible above and below the vein. Sample 168-1027C-1R-2, Piece 1A. **2.** CL image of the same vein as shown in Figure 1. Clay has no CL and appears black. Calcite CL is zoned and shows successive growth stages of the calcite vein fill. **3.** Plane-light photograph of a blocky aragonite vein with a clay selvage (brown) attached to a basalt sample. The area to the left of the aragonite is epoxy; however, the vein was probably originally symmetrical, with a thin clay selvage at the left edge as well. Sample 168-1032A-12R-3, Piece 5. **4.** CL image of the same vein as shown in Figure 3. The CL color and intensity of aragonite varies from yellow-green to deep orange to black, and the yellow-green zone is enriched in Sr.